tvst

https://doi.org/10.1167/tvst.7.3.6

Article

Liquid Biopsy of Vitreous Reveals an Abundant Vesicle Population Consistent With the Size and Morphology of Exosomes

Yuanjun Zhao[1], Sarah R. Weber[1,2], Joshua Lease[3], Mariano Russo[4], Christopher A. Siedlecki[5,6], Li-Chong Xu[5], Han Chen[7], Weiwei Wang[1], Michael Ford[8], Rafael Simó[9], and Jeffrey M. Sundstrom[1,2]

[1] Department of Ophthalmology, Penn State Hershey Medical Center, Hershey, PA, USA
[2] Kellogg Eye Center, University of Michigan, Ann Arbor, MI, USA
[3] Research Informatics, Penn State Hershey Medical Center, Hershey, PA, USA
[4] Department of Biochemistry and Molecular Biology, Penn State Hershey Medical Center, Hershey, PA, USA
[5] Department of Surgery, Penn State Hershey Medical Center, Hershey, PA, USA
[6] Department of Biomedical Engineering, Penn State Hershey Medical Center, Hershey, PA, USA
[7] Microscopy Imaging Facility, Penn State Hershey Medical Center, Hershey, PA, USA
[8] MS Bioworks LLC, Ann Arbor, MI, USA
[9] Institut de Recerca Hospital Universitari Vall d'Hebron (VHIR) and CIBERDEM (Instituto de Salud Carlos III), Barcelona, Spain

Correspondence: Jeffrey M. Sundstrom, Penn State Hershey Medical Center, Department of Ophthalmology, 500 University Dr, Hershey, PA 17033, USA. e-mail: jsundstrom@pennstatehealth.psu.edu

Received: 4 October 2017
Accepted: 3 March 2018
Published: 14 May 2018

Keywords: vitreous; exosomes; proteomics

Citation: Zhao Y, Weber SR, Lease J, Russo M, Siedlecki CA, Xu L-C, Chen H, Wang W, Ford M, Simó R, Sundstrom JM. Liquid biopsy of vitreous reveals an abundant vesicle population consistent with the size and morphology of exosomes. Trans Vis Sci Tech. 2018;7(3):6, https://doi.org/10.1167/tvst.7.3.6

Purpose: To investigate the molecular components of the vitreous in order to better understand retinal physiology and disease.

Methods: Vitreous was acquired from patients undergoing vitrectomy for macular hole and/or epiretinal membrane, postmortem donors, and C57BL/6J mice. Unbiased proteomic analysis was performed via electrospray ionization tandem mass spectrometry (MS/MS). Gene ontology analysis was performed and results were confirmed with transmission electron microscopy, atomic force microscopy, and nanoparticle tracking analysis (NTA).

Results: Proteomic analysis of vitreous obtained prior to vitrectomy identified a total of 1121 unique proteins. Gene ontology analysis revealed that 62.6% of the vitreous proteins were associated with the gene ontology term "extracellular exosome." Ultrastructural analyses, Western blot, and NTA confirmed the presence of an abundant population of vesicles consistent with the size and morphology of exosomes in human vitreous. The concentrations of vitreous vesicles in vitrectomy patients, postmortem donors, and mice were 1.3, 35, and 9 billion/mL, respectively.

Conclusions: Overall, these data strongly suggest that information-rich exosomes are a major constituent of the vitreous. The abundance of these vesicles and the presence of retinal proteins imply a dynamic interaction between the vitreous and retina. Future studies will be required to identify the cellular origin of vitreal exosomes as well as to assess the potential role of these vesicles in retinal disease and treatment.

Translational Relevance: The identification of vitreous exosomes lays the groundwork for a transformed understanding of pathophysiology and treatment mechanisms in retinal disease, and further validates the use of vitreous as a proximal biofluid of the retina.

Introduction

The vitreous body, a gel-like extracellular material, fills the posterior component of the eye. The vitreous is composed largely of collagen and hyaluronic acid and is generally considered to be protein deficient. However, recent investigations have detected an abundance of proteins in the vitreous, although the sources and purposes of these proteins are not yet understood. To gain insight into the origins and functional roles of vitreous proteins, we sought to examine 'normal' vitreous from vitrectomized, postmortem, and mouse eyes.

There is strong evidence that proteins within the vitreous can alter the state of several retinal diseases. Perhaps the most conspicuous example of this relationship is the widespread increase in intravitreal injections of anti–vascular endothelial growth factor (VEGF) ligands for the treatment of diabetic macular edema (DME)[1,2] and age-related macular degeneration (AMD)[3,4] over the last decade. Although this intervention is now the standard of care and has revolutionized the treatment of DME and AMD, less than half of patients respond with modest improvements in visual acuity, suggesting the presence of pathological changes other than alterations in VEGF signaling. In this context, proteomic analysis of the vitreous may provide valuable insight into the molecular underpinnings of retinal disease, reveal new therapeutic targets, and allow more reliable predictions of patients' responses to treatment.

The gel-like vitreous begins to liquefy early in life by a process known as liquefaction, and by the age of 18 roughly 20% of the vitreous is in the liquefied form.[5] Liquefaction continues with age and results in a posterior vitreous detachment in the majority of individuals over 50 years of age.[6] Anomalous vitreous detachments (AVDs) occur when the vitreoretinal interface is disrupted during the liquefactive process. Macular hole (MH) formation, vitreomacular traction, and epiretinal membrane (ERM) formation represent a continuum of vitreoretinal diseases that occur secondary to AVDs.[7]

Numerous studies using mass spectrometry (MS)-based methods have analyzed MH/ERM and postmortem vitreous in an effort to define the 'normal' vitreous proteome and to better understand its potential function following ocular development; over 1000 vitreous proteins have been identified by these studies thus far. One such study, by Kim et al.,[8] identified 346 vitreous proteins using pooled vitreous samples from patients with MH. Additionally, a study by Aretz et al.[9] using trichloroacetic acid/acetone precipitation combined with isoelectric focusing (IEF) and/or sodium dodecyl sulfate polyacrylamide gel electrophoresis (SDS-PAGE) of both soluble and precipitated proteins led to the identification of 1111 nonredundant proteins in vitreous samples from three ERM patients. In another study, by Murthy et al.,[10] pooled vitreous samples from patients with MH, congenital cataract, and trauma were subjected to prefractionation using strong-cation exchange as well as IEF to identify 1205 proteins. Most recently, Skeie et al.[11] identified over 2000 proteins in each of four anatomic vitreous compartments in postmortem human vitreous from nondiseased eyes using high-performance liquid chromatography (HPLC) coupled with electrospray ionization (ESI)-MS/MS.[1] These studies are more fully reviewed by Rocha et al.[12] While these techniques yield a much larger number of proteins identified in vitreous, the prefractionation methods remain complex and the required sample volumes are excessive, making proteomic analysis of individual samples challenging. Further, despite the breadth of data generated by these investigations, a meaningful conceptual framework for understanding vitreous function has yet to emerge.

The goal of the current study was to further study the vitreous proteome across multiple models in order to gain insight into the origin and function of normal vitreous proteins. Vitreous samples were obtained from the following three sources: patients undergoing pars plana vitrectomy for MH repair and/or ERM peel, postmortem human donors with no known ocular pathologies, and C57BL/6J mice. Proteomic analysis, ultrastructural imaging, and NTA suggest that exosomes are a normal constituent of vitreous. These extracellular vesicles contain protein, messenger RNA, and micro (mi)RNA and play a critical role in cell–cell communication.[13–16]

Methods

Subjects

Vitrectomy Samples

This study was approved by the University of Michigan institutional review board (IRB) and adhered to the tenets of the Declaration of Helsinki. The vitreous samples were collected in the operating room before clinically indicated vitrectomy as part of a larger protocol establishing a vitreous biorepository at the University of Michigan. Each patient in the

study had a vitreoretinal condition resulting from AVD (Supplementary Data: Vitrectomy Patient Demographics). Sequential samples obtained on August 23, 2012 and November 22, 2013 were analyzed as part of the current study. Briefly, the patient was taken to the operating room and either general or local anesthesia was induced. Trocars were used to place two cannulas in the usual fashion. With the infusion off, the microvitrector was placed into the midvitreous cavity. The surgical assistant applied gentle aspiration to an attached 3-mL syringe. At this time, approximately 0.25-mL vitreous fluid was collected. The syringe was placed on wet ice and immediately transported to a −80°C freezer adjacent to the operating room suite.

Postmortem Samples

IRB approval was obtained for this study from Vall d'Hebron University Hospital. This study adheres to all the tenants of the Declaration of Helsinki. Postmortem retinal tissue was acquired from Blood and Tissue Bank of Vall d'Hebron University Hospital. To be included in this study, an ophthalmoscopic examination must have been performed within 2 years prior to death, documenting the absence of ophthalmic disease. Vitreous was collected by careful suction using an automatic micropipette and immediately frozen at −80°C. The average death to harvest time was 3.8 hours.

Mouse Samples

Vitreous was isolated as described by Skeie et al.[17] Briefly, C57BL/6J mice were euthanized and globes were removed. The anterior segment was dissected using a circumferential incision at the limbus. The lens was elevated using a curved needle holder to facilitate removal with adherent vitreous. The lens-vitreous-retina sample was placed onto a filtration tube along with 20 µL of protease inhibitor cocktail (Roche Diagnostics Corporation, Indianapolis, IN) dissolved in phosphate buffer solution (PBS), then spun at 14,000*g* for 12 minutes.

Mass Spectrometry

Electrospray ionization MS/MS was conducted with a Waters nano-HPLC coupled with a Thermo Fisher Orbitrap Velos Pro mass spectrometer or QExactive instrument (Waters Corporation, Millford, MA; Thermo Fisher Scientific, Waltham, MA). Briefly, 90 µL of each sample was pooled and subjected to further analysis prior to or after abundant protein removal using the Multiple Affinity Removal System (specific for the 14 most abundant human plasma proteins; P/N5188-6560; Agilent Technologies, Santa Clara, CA). Abundant protein removal was carried out per the vendor protocol. A total of 20 µg of protein-depleted sample was processed using SDS-PAGE with a 4% to 12% Bis-Tris gel (Thermo Fischer Scientific) using the 3-(N-morpholino)propanesulfonic acid buffer system. Each gel lane was excised into 20 or 40 equal-sized segments and digested in-gel with trypsin. Trypsin digestion was performed using a ProGest robot (DigiLab, Inc, Marlborough, MA). Briefly, fragments were washed with 25 mM ammonium bicarbonate followed by acetonitrile, reduced with 10 mM dithiothreitol at 60°C followed by alkylation with 50 mM iodoacetamide at room temperature, digested with sequencing grade trypsin (Promega, Madison, WI) at 37°C for 4 hours, then quenched with formic acid. The supernatant was analyzed directly without further processing. Peptides were loaded on a trapping column and eluted over a 75-µm analytical column at 350 nL/min; both columns were packed with Jupiter Proteo resin (Phenomenex, Torrance, CA). The injection volume was 30 µL. Each mass spectrometer was operated in data-dependent mode, with the Orbitrap operating at 60,000 and 17,500 FWHM for MS and MS/MS, respectively.

Data Analysis

The 15 most abundant ions were selected for MS/MS. Data were searched using the Mascot search engine with the SwissProt Human (forward and reverse appended with common contaminant proteins) database set to carbamidomethyl (C) fixed modification. Variable modification parameters were set to oxidation (M, Acetyl [N-term], Pyro-Glu [N-term Q]) and deamidation (N, Q). The peptide mass tolerance was set to 10 ppm and the fragment mass tolerance was set to 0.02 Da. A maximum of two missed cleavages and at least two unique peptides were required for protein identification. The false discovery rate was calculated for each MS experiment and is reported in Supplementary Data (MS Experiments). The resulting mass spectra were searched against the SwissProt database using Mascot (SwissProt_Human; forward and reverse; appended for common contaminant proteins), and the resultant Mascot DAT files were parsed into Scaffold (Proteome Software, Portland, OR) for validation, filtering, and generation of nonredundant identifications. Gene Ontology (GO) analysis was conducted using GO Enrichment (geneontology.org). During the

process of uploading protein identifications, proteins identified in Scaffold with ambiguous association to genes in the Ingenuity Pathway Analysis database were excluded from the analysis.

Exosome Isolation

Exosome enrichment was performed using ExoQuick (System Biosciences, Palo Alto, CA). Approximately 250 μL (450 μg protein) of vitreous fluid was centrifuged at 2000*g* for 30 minutes at 4°C, resulting in a small pellet (P1). The initial supernatant (S1) was centrifuged at 12,000*g* for 30 minutes at 4°C, resulting in a second pellet (P2) containing cellular and vitreous debris, and a supernatant (S2) containing 'buoyant' vesicles. According to manufacturer's instructions, 63 μL ExoQuick reagent was added to the S2 fraction, mixed well, and incubated at 4°C overnight. The mixture was then centrifuged at 1500*g* for 30 minutes at 4°C to separate pellet from supernatant (S3). The pellet was centrifuged at 1500*g* for another 5 minutes at 4°C to yield the pellet (P3, exosomes) and residual supernatant.

As a positive control for some of the exosome markers, we used exosomes derived from human retinal pigment epithelial cells (ARPE-19) expressing inducible wild-type fibulin-3-eGLuc2. These cells were not induced with doxycycline and the transgene was not expressed. These cells were obtained from Dr. John D Hulleman[18] at University of Texas Southwestern Medical Center and cultured in Dulbecco's modified Eagles medium/Ham's F12 50/50 mix (DMEM/F12; Corning, Manassas, VA) supplemented with 10% fetal bovine serum (Gemini Bio Products, West Sacramento, CA) and Penn/Strep antibiotics (Corning) at 37°C and 5% CO_2. Cells were seeded in 145-mm dishes until 60% confluent, then media was removed and cells were washed three times with PBS and cultured in serum-free DMEM/F12 for 2 days. Approximately 30-mL media was harvested, filtered by a 0.22-μm membrane, and concentrated to 0.6 mL using Amicon Ultra-15 Centrifugal Filter Unit (3K MWCO; Millipore Sigma, Burlington, MA). One hundred fifty microliters of ExoQuick reagent was added to concentrated culture medium, mixed well, incubated at 4°C overnight, and the exosomes were fractionated as described above.

Transmission Electron Microscopy (TEM)

Cell lysates or exosome pellets from vitreous fluid (P1, P2, and P3) were fixed in half strength Karnovsky fixative (2% paraformaldehyde, 2.5% glutaraldehyde, pH 7.3) for 3 hours at 4°C. The samples were then washed with 0.1 M sodium cacodylate buffer, stained overnight with osmium tetroxide/potassium ferrocyanide, washed, and dehydrated with ethanol and propylene oxide before embedding in Epon 812. Ultrathin sections were stained with uranyl acetate and lead citrate prior to visualization.

Negative staining was conducted by adapting the protocol used by Théry et al.[19] Briefly, the supernatant (S2) and the resuspended pellet (P3) described above were fixed in 2% paraformaldehyde. The fixed vesicles (10 μL) were deposited on Formvar carbon-coated TEM grids and incubated for 20 minutes. The grids were then washed with PBS, incubated with glutaraldehyde, and washed with water. The vesicles were then stained with uranyl acetate solution and air dried. Vesicles were observed using the JEM1400 TEM (JEOL Ltd., Tokyo, Japan).

Atomic Force Microscopy (AFM)

A small volume of the S1, S2, and PBS resuspended P1, P2, and P3 fractions described above was placed on a mica substrate and allowed to air dry at room temperature. The sample was washed with ultrapure water to remove salts and dried with nitrogen gas. The sample was viewed using a Multimode AFM with a Nanoscope IIIa control system (software version 5.12r3; Veeco, Santa Barbra, CA) in tapping mode in air using Si probes having an aspect ratio of approximately 4:1 (TETRA, K-Tek Nanotechnology, Wilsonville, OR) in air. Images were acquired and analyzed with off-line AFM software.

Western Blot

Immunoblotting was performed as follows. Briefly, samples were heated at 70°C for 15 minutes in NuPAGE LDS sample buffer (Thermo Fisher Scientific) with 0.1 M dithiothreitol (except when probing with CD63 and CD81 antibodies), then separated on NuPAGE 4-12% Bis-Tris gel (Thermo Fisher Scientific) and transferred in NuPAGE transfer buffer (Thermo Fisher Scientific) with 20% methanol and 0.05% SDS to a NitroBind 0.45-μm nitrocellulose membrane (GVS Maine, Sanford, ME). The membrane was blocked in 5% nonfat milk dissolved in tris-buffered saline with Tween (TBST) (10 mM Tris, 150 mM NaCl, 0.05% Tween-20, pH 7.2) for 1 hour at room temperature, then incubated with primary antibodies (Supplementary Data: Primary Antibodies) diluted in blocking buffer at 4°C overnight. The membrane was washed 4 times for 10 minutes each

time in TBST, incubated for 2 hours at room temperature with secondary antibodies (alkaline phosphatase conjugated goat anti-mouse IgG + IgM or goat anti-rabbit IgG; Jackson ImmunoResearch, West Grove, PA) diluted in blocking buffer, then washed another 4 times in TBST for 10 minutes each time. Signals were detected by Vistra ECF Substrate (GE Healthcare; Little Chalfont, UK). Images were scanned by Typhoon 9400 (GE Healthcare).

Nanoparticle Tracking Analysis

Vitreous samples were removed from storage at −80°C, thawed on ice, and centrifuged at 2000*g* for 30 minutes at 4°C. The supernatants were diluted to 1 mL (1:50 to 1:1000) with particle-free water. Each sample was loaded by syringe pump into the NanoSight NS300 (Malvern Instruments Ltd, Malvern, Worcestershire, UK) set in scatter mode, and five 60-second videos were generated at 24.98 frames/sec. The size distribution and concentration of particles were calculated and images were acquired using NanoSight software version 3.2 (Malvern Instruments Ltd). The same individual ran all samples in the current data set on the same day.

The raw NanoSight data were analyzed using Microsoft Excel algorithms (Redmond, WA). The algorithm used identified all 'peaks' across the entire size spectrum (1–1000 nm parsed into 1-nm bins). For this study, peaks were operationally defined as a nanometer value, n, whose vesicle concentration value was greater than both n − 1 and n + 1. Only peaks accounting for >5% of the total vesicle population were considered for further analysis. For each such peak, the total vesicle abundance of the peak was calculated by adding the vesicle concentrations of nanometer values ranging from n − 5 to n + 5. This range was chosen because the standard deviation across all NanoSight runs was approximately 11 nm.

Results

Mass Spectrometry Overview

Vitreous was digested and subjected to ESI-MS/MS experiments using either a qExactive or Orbitrap Velos instrument, with the SDS-PAGE excised into either 20 or 40 equal-sized fragments. A nonredundant list of 1121 proteins was generated by combining the data from these experiments, as detailed in Supplementary Data (MS Experiments). A comparison of the proteins identified before and after abundant protein removal revealed that 89 proteins were identified before, but not after, depletion. An additional 360 proteins were identified after abundant protein depletion. There were 447 proteins identified with both methods. A complete list of peptides and proteins identified in these studies is available for download (Supplementary Data: Peptide Report; Protein Report; Nonredundant Protein List).

Gene Ontology Analysis of Vitreous Proteins

GO analysis was performed using the Enrichment Analysis algorithm on the GO website (http://geneontology.org/). Analysis was conducted independently for each GO annotation arm (Cellular Component, Molecular Function, Biological Process). Figure 1 shows the percentage of proteins for each of the top 25 most enriched GO terms. A more detailed list of the top 25 GO terms for each category is shown in Supplementary Data (GO Website_Table_Top25). The most striking pattern observed in this analysis was that over 60% of AVD vitreous proteins mapped to the GO term "Extracellular Exosomes" in the Cellular Component arm of the analysis. The Molecular Function and Biological Function GO arms did not yield any significant patterns. Given that vesicles and related structures were prevalent in the GO analysis, the distribution of terms specific to various organelle vesicles/structures was assessed (Fig. 2). The National Center for Biotechnology Information (NCBI) GO term 'extracellular exosome' was associated with 702 of the vitreous proteins (62.6%). Other organelle GO terms such as 'Golgi apparatus', 'endosome', and 'peroxisome' were poorly represented. In order to confirm these results, the well-curated exosome protein list from ExoCarta[20] was compared with the current vitreous fluid data set. This analysis revealed that more than a third (448/1121) of the vitreous proteins identified in the current study have been previously isolated in exosomes. Further, 47 of the top 100 proteins most frequently identified in exosomes (ExoCarta) were identified in the current study (Table 1). This information, together with the GO analysis described above, suggests that vitreous fluid from eyes with AVD may contain exosomes.

Isolation and Characterization of Vitreous Vesicles

Vitreous vesicles from postmortem vitreous were isolated as described in the Methods section (Fig. 3). Multiple fractions were imaged by AFM and TEM

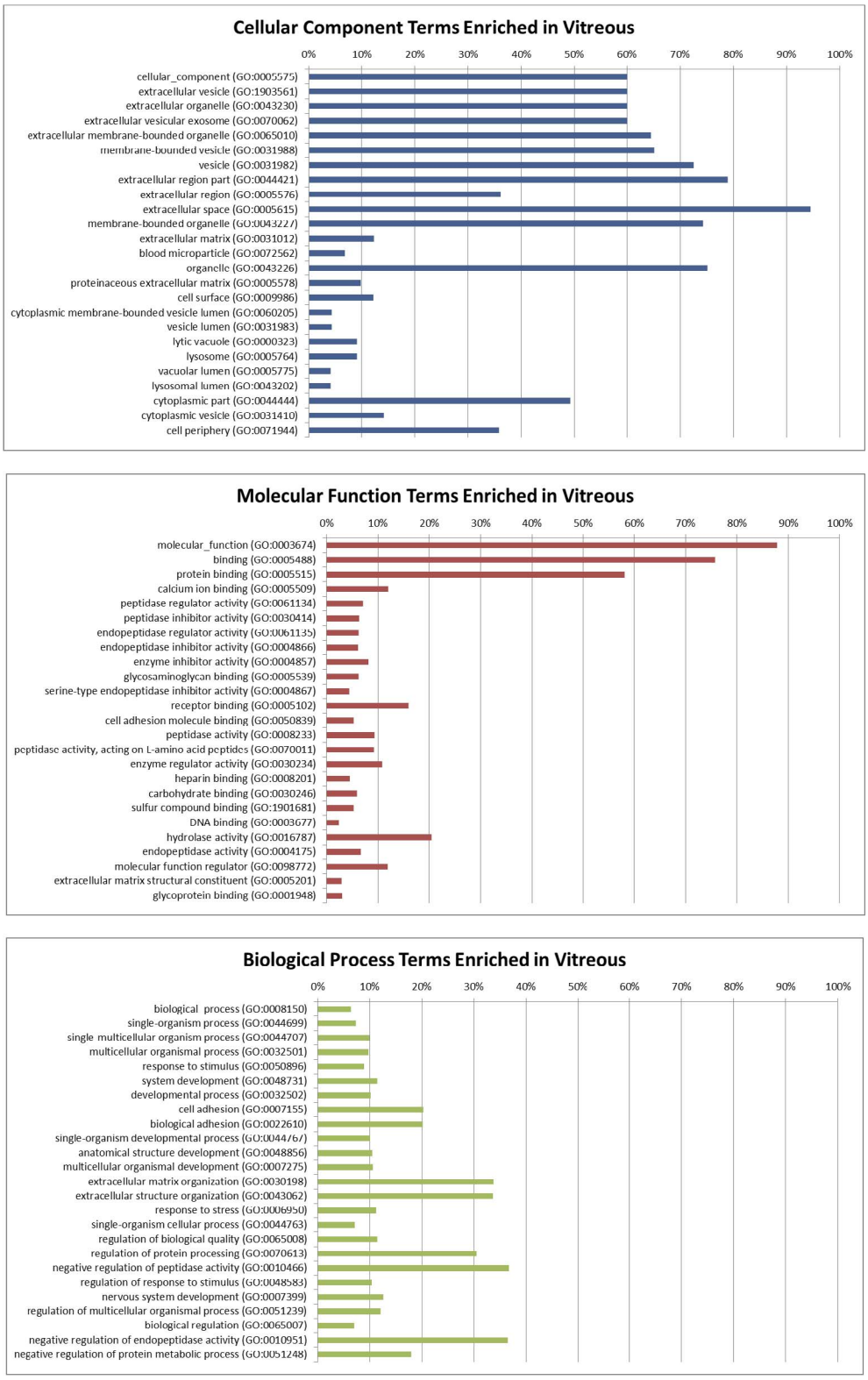

Figure 1. GO analysis of vitreous proteins. GO analysis was conducted using GO Enrichment (geneontology.org). Each of the three GO branches (Cellular Location, Molecular Function, and Biological Process) is graphed independently. Several 'Cellular Components' were noted to be enriched over 50% in vitreous including extracellular vesicular exosome. The 'Molecular Function' aspect of the analysis suggested enrichment for proteins involved in 'protein binding'. The 'Biological Process' aspect of the analysis did not identify any process enriched over 40%.

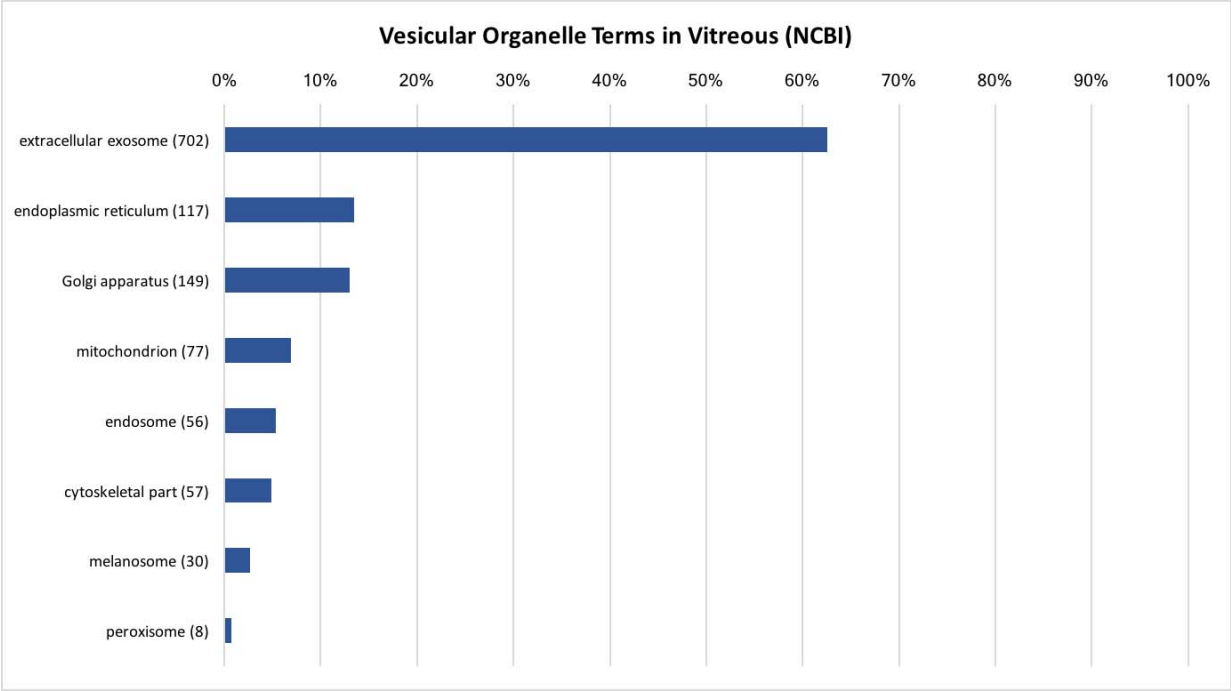

Figure 2. Distribution of vesicular organelle GO terms (NCBI) in vitreous proteome. The percentage of proteins associated with subcellular organelles as defined by NCBI. Of the 1121 proteins identified in vitreous, 702 (62.6%) have been identified in extracellular exosomes.

(Fig. 4). Following the initial fractionation (30 minutes at 2000*g*), AFM and TEM of the pellet (P1) revealed abundant cellular debris as well as arrays of fibers consistent with collagen fibrils known to be present in vitreous. AFM of the initial supernatant (S1) revealed an abundant population of vesicles approximately 100 nm in diameter. The S1 fraction was then fractionated further to obtain all subsequent images. After 30 minutes of centrifugation at 12,000*g*, the resulting P2 fraction revealed cellular debris of varying size and electron density, while imaging of the S2 fraction revealed a homogeneous population of vesicles approximately 100 nm in diameter. Following addition of the ExoQuick and final centrifugation, AFM and TEM of the vesicle-containing pellet (P3) again revealed 100-nm sized vesicles. Images obtained from S1, S2, and P3 fractions are similar in size and morphology to those obtained from exosomes isolated by others.[21,22]

To characterize extracellular vesicles visible on AFM and TEM, immunoblotting was performed on postmortem human vitreous samples from donors with no known ocular pathology (Fig. 5). Overall, the immunoblot analysis following exosome enrichment is consistent with the MS results. Specifically, heat shock 70 kDa protein (HSP70), glyceraldehyde-3-phosphate dehydrogenase (GAPDH), and Annexin V were identified in both nonfractionated vitreous by MS and Western blot analysis after exosome enrichment (P3). Programmed cell death 6-interacting protein (ALIX) and flotillin-1 were not detected in the MS and immunoblot analyses of nonfractionated vitreous. However, ALIX immunoreactivity was increased following exosome enrichment. Similarly, flotillin-1 immunoreactivity increased with exosome enrichment, but to a lesser extent (Fig. 5A). Immunoreactivities of Golgin subfamily A member (GM130), a Golgi protein; calnexin, an endoplasmic reticulum protein; histone H3, a nuclear protein; and mitochondrial import inner membrane translocase subunit TIM23 (TIM23), a mitochondrial protein, were minimal or undetectable, validating the exosomal preparation (Fig. 5B). CD63 antigen (CD63) and CD81 antigen (CD81), tetraspanins often used as exosomal markers, were not present in the vitreous exosome fraction. Exosomes derived from ARPE-19 cells were used as a positive control for the immunoblotting procedure (Fig. 5C). Taken

Table 1. Detection of Common Exosome Proteins in Vitreous

Number	Gene Symbol	UniProt Entry Name	Number of Times Identified	Presence (+) or Absence (−) in Vitreous Proteomics
1	*CD9*	CD9	98	−
2	*HSPA8*	HSP7C	97	+
3	*PDCD6IP*[a]	PDC6I	96	−
4	*GAPDH*[a]	G3P	95	+
5	*ACTB*	ACTB	93	−
6	*ANXA2*	ANXA2	83	+
7	*CD63*	CD63	82	−
8	*SDCBP*	SDCB1	78	−
9	*ENO1*	ENOA	78	+
10	*HSP90AA1*	HSP90A	77	−
11	*TSG101*	TS101	76	−
12	*PKM*	KPYM	72	−
13	*LDHA*	LDHA	72	+
14	*EEF1A1*	EF1A1	71	+
15	*YWHAZ*	1433Z	69	+
16	*PGK1*	PGK1	69	+
17	*EEF2*	EF2	69	+
18	*ALDOA*	ALDOA	69	+
19	*HSP90AB1*	HS90B	67	+
20	*ANXA5*[a]	ANXA5	67	+
21	*FASN*	FAS	66	+
22	*YWHAE*	1433E	65	+
23	*CLTC*	CLH1	64	−
24	*CD81*	CD81	64	−
25	*ALB*	ALBU	64	−
26	*VCP*	TERA	62	−
27	*TPI1*	TPIS	62	+
28	*PPIA*	PPIA	62	+
29	*MSN*	MOES	62	+
30	*CFL1*	COF1	62	+
31	*PRDX1*	PRDX1	61	+
32	*PFN1*	PROF1	61	+
33	*RAP1B*	RAP1B	60	−
34	*ITGB1*	ITB1	60	−
35	*HSPA5*	GRP78	58	+
36	*SLC3A2*	YF2	57	+
37	*HIST1H4A*	H4	57	+
38	*GNB2*	GBB2	57	−
39	*ATP1A1*	AT1A1	57	−
40	*YWHAQ*	1433T	56	+
41	*FLOT1*	FLOT1	56	−
42	*FLNA*	FLNA	56	−
43	*CLIC1*	CLIC1	56	+
44	*CDC42*	CDC42	56	−
45	*CCT2*	TCPB	56	−

Table 1. Continued

Number	Gene Symbol	UniProt Entry Name	Number of Times Identified	Presence (+) or Absence (−) in Vitreous Proteomics
46	*A2M*	A2MG	55	+
47	*YWHAG*	1433G	54	+
48	*TUBA1B*	TBA1B	53	−
49	*RAC1*	RAC1	53	−
50	*LGALS3BP*	LGAGLS3BP	53	+
51	*HSPA1A*[a]	HSP71	53	+
52	GNAI2	GNAI2	53	−
53	ANXA1	ANXA1	53	+
54	RHOA	RHOA	52	−
55	MFGE8	MFGM	52	−
56	*PRDX2*	PRDX2	51	+
57	*GDI2*	GDIB	51	+
58	*EHD4*	EHD4	51	−
59	*ACTN4*	ACTN4	51	−
60	*YWHAB*	1433B	50	+
61	*RAB7A*	RAB7A	50	−
62	*LDHB*	LDHB	50	+
63	*GNAS*	GNAS	50	−
64	*TFRC*	TFR1	49	−
65	*RAB5C*	RAB5C	49	−
66	*ARF1*	ARF1	49	−
67	*ANXA6*	ANXA6	49	−
68	*ANXA11*	ANXA11	49	−
69	*ACTG1*	ACTG	49	+
70	*KPNB1*	IMB1	48	−
71	*EZR*	EZRI	48	−
72	*ANXA4*	ANXA4	48	−
73	*ACLY*	ACLY	48	−
74	*TUBA1C*	TBA1C	47	−
75	*RAB14*	RAB14	47	−
76	*HIST2H4A*	H4	47	+
77	*GNB1*	GBB1	47	+
78	*UBA1*	UBA1	46	−
79	*THBS1*	TSP1	46	+
80	*RAN*	RAN	46	+
81	*RAB5A*	RAB5A	46	−
82	*PTGFRN*	FPRP	46	−
83	*CCT5*	TCPE	46	−
84	*CCT2*	TCPB	46	−
85	*BSG*	BASI	46	+
86	*AHCY*	SAHH	46	+
87	*RAB5B*	RAB5B	45	−
88	*RAB1A*	RAB1A	45	−
89	*LAMP2*	LAMP2	45	+
90	*ITGA6*	ITA6	45	−

Table 1. Continued

Number	Gene Symbol	UniProt Entry Name	Number of Times Identified	Presence (+) or Absence (−) in Vitreous Proteomics
91	*HIST1H4B*	H4	45	+
92	*GSN*	GELS	45	+
93	*FN1*	FINC	45	+
94	*YWHAH*	1433F	44	+
95	*TUBA1A*	TBA1A	44	−
96	*TKT*	TKT	44	+
97	*TCP1*	TCPA	44	−
98	*STOM*	STOM	44	−
99	*SLC16A1*	MOT1	44	−
100	*RAB8A*	RAB8A	44	−

Presence (+) or absence (−) in vitreous proteomics of the top 100 proteins identified in exosomes, as compiled by ExoCarta in an analysis of 286 studies. Of the top 100 proteins, the most frequently identified proteins are detected in exosomes approximately one-third of the time (98 times in 286 studies). Of the 100 proteins listed, 47 were detected in the current proteomic data.

[a] Proteins that were validated by immunoblot (PDCD6IP = ALIX, GAPDH; HSPA1A = HSP70; ANXA5 = Annexin V).

together, these results strongly suggest that a distinct population of tetraspanin-negative exosomes is present in the vitreous.

Quantitative Nanoparticle Tracking Analysis of Unfractionated Vitreous

NTA was performed on MH/ERM, postmortem, and mouse vitreous samples to quantify the abundance of extracellular vesicles and their size distribution. It should be noted that the average diameter of vesicles as determined by NTA is larger than the same measurement on TEM or AFM. This is likely due to dehydration of the vesicles by staining during the preparation of samples for microscopy (in contrast to the NTA sample preparation, in which no staining was performed). NTA of unfractionated MH/ERM vitreous humor ($n = 8$) revealed an average sample particle size of 160 nm across all peaks. The average particle size for the dominant peaks in each sample (any peak that constituted >5% of data) was 125 nm. Similar results were obtained when analyzing human postmortem and mouse vitreous, with average particle diameters of 114 and 128 nm, respectively (Table 2). Interestingly, despite similar vesicle size, the three sample types differed greatly in their vesicle concentrations, with the greatest difference being a 27-fold increase in average exosome concentration (Table 2) in postmortem human samples relative to MH/ERM human samples. Mouse vitreous showed a particle concentration intermediate to that of MH/ERM and postmortem human samples. Representative graphs of vesicle concentration versus size are shown for MH/ERM, postmortem, and mouse samples in Figure 6. In addition, videos of representative nanoparticles in postmortem (Supplementary Movie S1), mouse (Supplementary Movie S2), and MH/ERM (Supplementary Movie S3) samples are available in the Supplementary Data.

Identification of Proteins Associated With Retinal Disease in Vitreous

In order to more fully determine if vitreous biopsy can be used to identify proteins associated with retinal disease, we queried the Online Mendelian Inheritance in Man (OMIM) database (http://www.ncbi.nlm.nih.gov/omim) using the key words "Retinal Disease." This query resulted in 655 "Retinal Disease" genes/proteins. We then compared this list of proteins with the current study and identified 86 proteins found in vitreous and associated with "Retinal Disease" in OMIM. After manual verification of these 86 retinal disease proteins, we determined that 42 of 86 proteins had a well-documented role in retinal disease. Analysis of this list of 42 proteins led to the following conclusions. Firstly, plasma proteins associated with retinal disease are readily detectable in vitreous (numerous complement

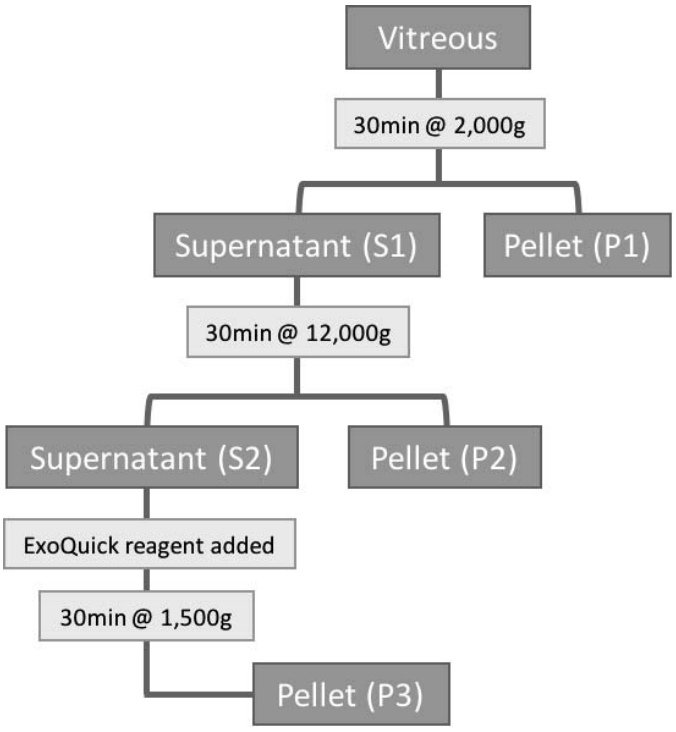

Figure 3. Exosome isolation protocol. Vitreous was centrifuged at 2000*g* for 30 minutes, yielding a small pellet (P1). The initial supernatant (S1) was centrifuged at 12,000*g* for 30 minutes to yield a second pellet (P2) containing cellular and vitreous debris, and a supernatant (S2) containing 'buoyant' vesicles. ExoQuick reagent was added to the S2 fraction and the ExoQuick protocol was followed, yielding the exosome pellet (P3).

factors, apolipoprotein E (APO-E), and kininogen). In addition, the identification of retinoschisin and S-arrestin suggest that proteins expressed by the neural retina are detectable in vitreous. Identification of VEGF, VEGF-receptor(R)1, epithelial discoidin domain-containing receptor 1 (DDR1), and EGF-containing fibulin-like extracellular matrix protein 1 (EFEMP1) suggest that proteins expressed by the retinal pigment epithelium (RPE) are also detectable in vitreous. Further, we found that of the 42 confirmed retinal disease proteins identified in vitreous, 20 had been previously identified in exosomes (ExoCarta), including complement factor H, EFEMP1, myocilin, and VEGF-R1. That nearly half of the vitreal proteins known to play a role in retinal disease are also found in exosomes raises important questions about the potential role of these vesicles in retinal disease. Taken together, these data suggest that the vitreous contains proteins derived from plasma, neuroretina, and RPE that are associated with retinal disease, and that exosomes may play a role in the disease process. A list of well-studied proteins supporting this conclusion is shown in Table 3.

Discussion

The goal of the present study was to conduct an in-depth proteomic analysis of vitreous humor in order to gain insight into the role of the vitreous in ocular physiology and pathophysiology. Vitreous from patients diagnosed with MH and/or ERM occurring secondary to AVD was used to approximate 'normal' human vitreous. Using multiple preparative methods, we derived a nonredundant list of 1121 vitreous proteins in patients with MH/ERM. Vesicles were characterized by ultrastructural imaging and quantified by NTA, and the results together suggested the presence of exosomes in the vitreous humor of patients with AVD. Subsequent analysis of postmortem vitreous from human donors with no known ocular pathologies and mouse vitreous revealed vesicles consistent with the size distribution observed in vitreous from vitrectomized eyes. Taken together, these results suggest that exosomes are constitutively present as a component of vitreous in healthy eyes.

Extracellular vesicles can be classified into three subcategories: exosomes, apoptotic blebs (ABs), and shedding microvesicles (SMVs). The term 'exosome' refers to extracellular vesicles of endosomal origin that are secreted by the fusion of multivesicular bodies with the plasma membrane of the cell.[16,23] This is in contrast to ABs (vesicles released by the transient blebbing of the plasma membrane in apoptotic cells)[24] and SMVs (formed directly by budding of the plasma membrane).[16] Exosomes can also be differentiated from ABs and SMVs by their uniformity in size, lipid composition, and associated proteins.

To our knowledge, the current study is the first to determine the size distribution and abundance of vitreous vesicles across three different control groups to account for artifacts inherently present in each sample type. MH/ERM samples obtained using a vitrector contained an average of 1.3 billion vesicles/mL; postmortem vitreous samples obtained via needle aspiration contained an average of 35 billion vesicles/mL; and mouse vitreous obtained by gross dissection contained an average of 9 billion vesicles/mL. The immense number of exosomes observed across vitreous from multiple sources suggests a role for these vesicles in normal physiology as well as pathophysiology. The substantially greater exosome concentration in the postmortem samples is likely

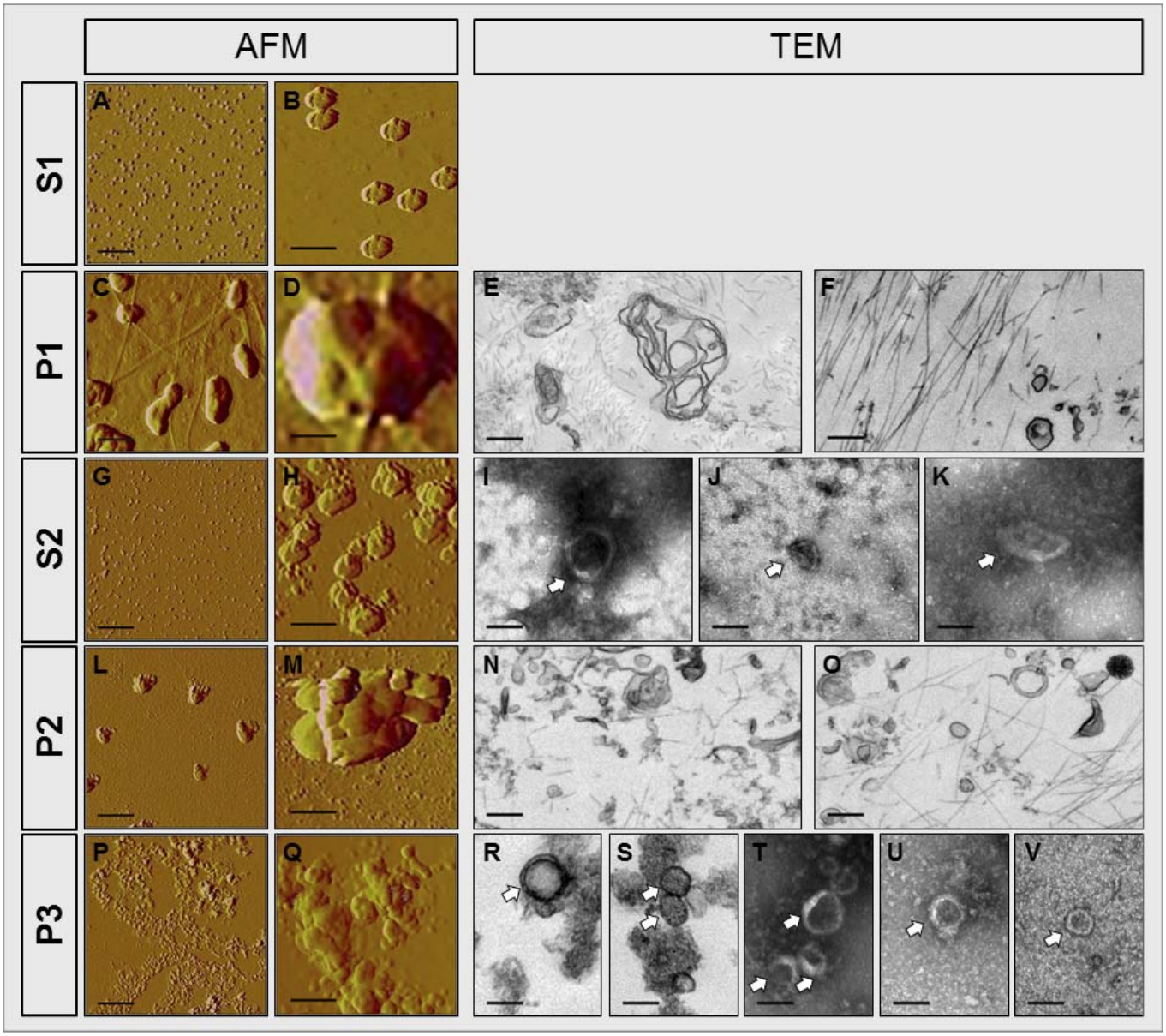

Figure 4. AFM and TEM images of vitreous fractions. AFM (*left*) and TEM (*right*) images are shown for vitreous fractions. No TEM images were obtained for S1. Cellular debris is visible in the P1 and P2 images. Exosomes are best visible in S1 (before the addition of ExoQuick) due to their naturally high abundance in the vitreous. Exosomes are also visible in the S2 and P3 fractions. Polymer from the ExoQuick reagent is visible in P3 *images R and S*; *arrows* indicate exosomes in these images. *Images T–V* were resuspended, ridding exosomes of excess polymer. *Scale bars*: (A, C, G, L, P): 1 μm; (B, D, H, M, Q): 200 nm; (E, F): 200 nm; (I–K): 100 nm; (N, O): 200 nm; (R–V): 100 nm.

secondary to poor perfusion and ischemia in the approximately 4 hours between death and tissue harvesting. Despite the significant variation in concentration, the consistency in vesicle diameter in samples across the three study groups suggests a normally present, ample exosome population.

Interestingly, vitreous exosomes appear to be distinct from other populations of exosomes in terms of their protein content. As shown in the Results section, vitreous vesicles lack the traditional exosome markers, CD63, CD81, and TSG101. Our data are consistent with prior proteomic studies on unfractionated vitreous that did not detect CD63, CD9, CD81, and TSG101.[11] Similarly, ALIX, CD63, CD9, and CD81 were absent in a similar study by Murthy et al.[10] It is well established that exosomes are heterogeneous in nature and their composition depends in large part on their cell of origin. In fact, even the most

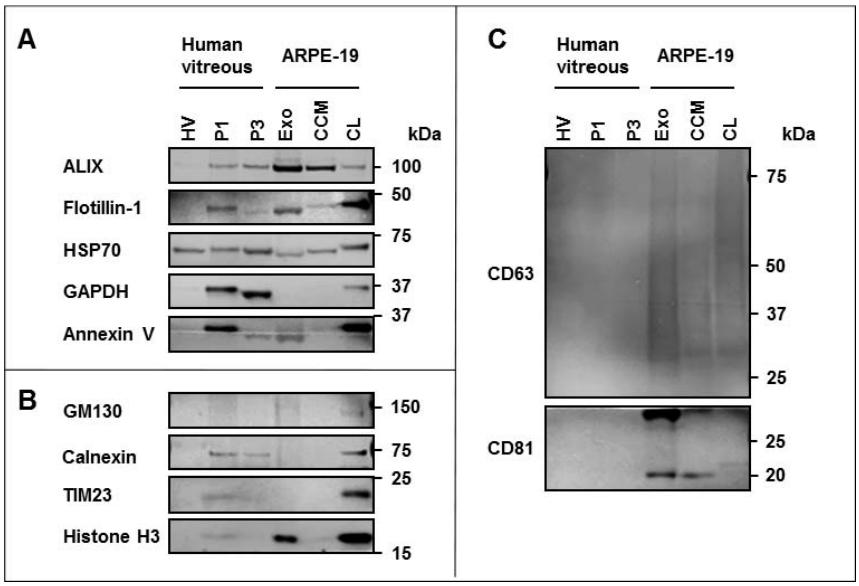

Figure 5. Western blot analysis of exosome fraction. Western immunoblotting was performed on unfractionated postmortem human vitreous (HV), the cellular debris fraction of vitreous (P1), and the fraction of vitreous containing exosomes (P3). Exosomes derived from ARPE-19 cell culture (Exo), conditioned media from these cells (CCM), and whole cell lysates (CL) are shown for comparison. (A) The exosome fraction of human vitreous (P3) is positive for exosomal proteins ALIX, HSP70, GAPDH, and Annexin V. Flotilin-1, which is variably found in exosomes, was weakly detected. (B) Purity of vitreous exosomes were confirmed using the following organelle markers: GM 130 (a Golgi apparatus), calnexin (endoplasmic reticulum), histone H3 (nucleus), and TIM23 (mitochondria). (C) Traditional exosome markers CD63 and CD81 were absent from vitreous exosomes and present in ARPE-19-derived exosomes.

commonly identified exosome marker, CD9, is present in only 34% of the studies compiled and curated on the exosome database ExoCarta.

In a prior report by Ragusa et al.,[25] exosomes were identified in vitreous from uveal melanoma patients and postmortem controls. In their study, the average particle size of vitreous vesicles from melanoma patients was found to be approximately 100 nm using a Zetasizer, an instrument that is similar to the NanoSight NS300 used in the current study in that it can measure nanoparticle size. In contrast to the NanoSight, however, the Zetasizer is not capable of quantifying particle concentration. Further, although postmortem vesicles in the Ragusa et al.[25] study were purified, they were not subjected to Zetasizer analysis.

Additional studies of ocular exosomes have largely focused on tissues other than the vitreous. Exosomes were recently identified in aqueous humor[26,27] and subsequent studies have focused on the functional effects of nonpigmented ciliary epithelium–derived exosomes on trabecular meshwork cells[28] as well as the regulation of exosome release from trabecular meshwork cells grown in culture.[29] Multiple studies have also detailed the functions and characteristics of exosomes derived from RPE cells,[30–32] while another study identified exosomes in tears.[33]

Basic questions remain in terms of the cellular origin and physiologic function(s) of these vesicles. It seems most likely that vitreous exosomes are derived from the resident cells of the vitreous (hyalocytes), and/or from the tissues and cells types in close proximity to the vitreous. Anteriorly, these tissues include the lens and the ciliary body, the latter of which has been hypothesized to be the source of exosomes present in aqueous humor[26] and recently been shown to secrete exosomes in cell culture.[28] Posteriorly, the retina approximates the vitreous. Within the retina, the ganglion cells and endplates of Müller cells are in close proximity to the vitreous. Given that exosomes have been shown to facilitate immune cell communication, it also remains possible that microglia within the retina may generate exosomes that subsequently come to reside in the vitreous. The RPE lies posterior to the retina and may also play a role in vitreous exosome production, as vesicles similar in content to those found in aqueous humor have been identified in RPE cell culture.[27] Most likely, several of these cells/tissues play a role in vitreous exosome synthesis, and it seems reasonable to suspect that the population of these vesicles is extremely heterogeneous.

In addition to being secreted by a diverse array of

Table 2. Summary of NTA Data

Sample Type	Particle Diameter, nm	Concentration, 10^8 particles/mL	Percentage of Total Vesicles	Total Percentage of Peaks >5%
MH/ERM	80	4.8	7.1	37.0
	91	5.1	7.6	
	115	8.5	12.6	
	155	6.5	9.7	
MH/ERM	98	9.1	6.6	19.2
	147	17.4	12.6	
MH/ERM	95	28.4	20.4	30.9
	122	14.5	10.5	
MH/ERM	98	21.9	16.1	33.7
	116	17.4	12.8	
	166	6.5	4.8	
MH/ERM	117	16.2	13.9	13.9
MH/ERM	96	15.3	16.6	16.6
MH/ERM	93	22.1	19.0	39.0
	126	13	11.2	
	167	10.2	8.8	
MH/ERM	116	7.6	6.0	19.2
	160	10.1	8.0	
	230	6.7	5.3	
PM	80	205.2	4.6	28.7
	105	766.2	17.0	
	152	319.1	7.1	
PM	110	415.7	15.6	15.6
PM	92	129.9	8.0	22.3
	126	230.4	14.3	
PM	134	230.4	14.3	29.6
	115	525.9	15.3	
M	114	64.8	8.3	15.8
	178	58.5	7.5	
M	121	138.4	9.0	16.2
	152	110.5	7.2	
M	73	205.3	19.0	19.0
M	91	25.3	5.1	28.2
	128	84.6	17.1	
	169	29.5	6.0	

NTA data for MH/ERM human vitreous, postmortem human vitreous, and mouse vitreous. All peaks accounting for >5% of a given sample's data are shown. AUC,[10] area under curve; PM, postmortem; M, mouse.

healthy cell types across multiple systems, it is important to note that exosomes have been implicated in a number of pathological processes, including host infection by pathogens,[34,35] Alzheimer's Disease,[36–38] and tumor growth and metastasis in a variety of cancer types.[39–42] Because we are concerned with the role of the vitreous in retinal disease, the possibility that exosomes are at least in part derived from the abutting retina and RPE merits further discussion. This would result in the translocation of retinal and RPE proteins into the vitreous, an effect that is supported by the current findings. Specifically, our analysis suggests that 42 proteins associated with "Retinal Disease" by OMIM can be identified in the vitreous, including proteins central to AMD, diabetic retinopathy (DR), and multiple retinal dystrophies.

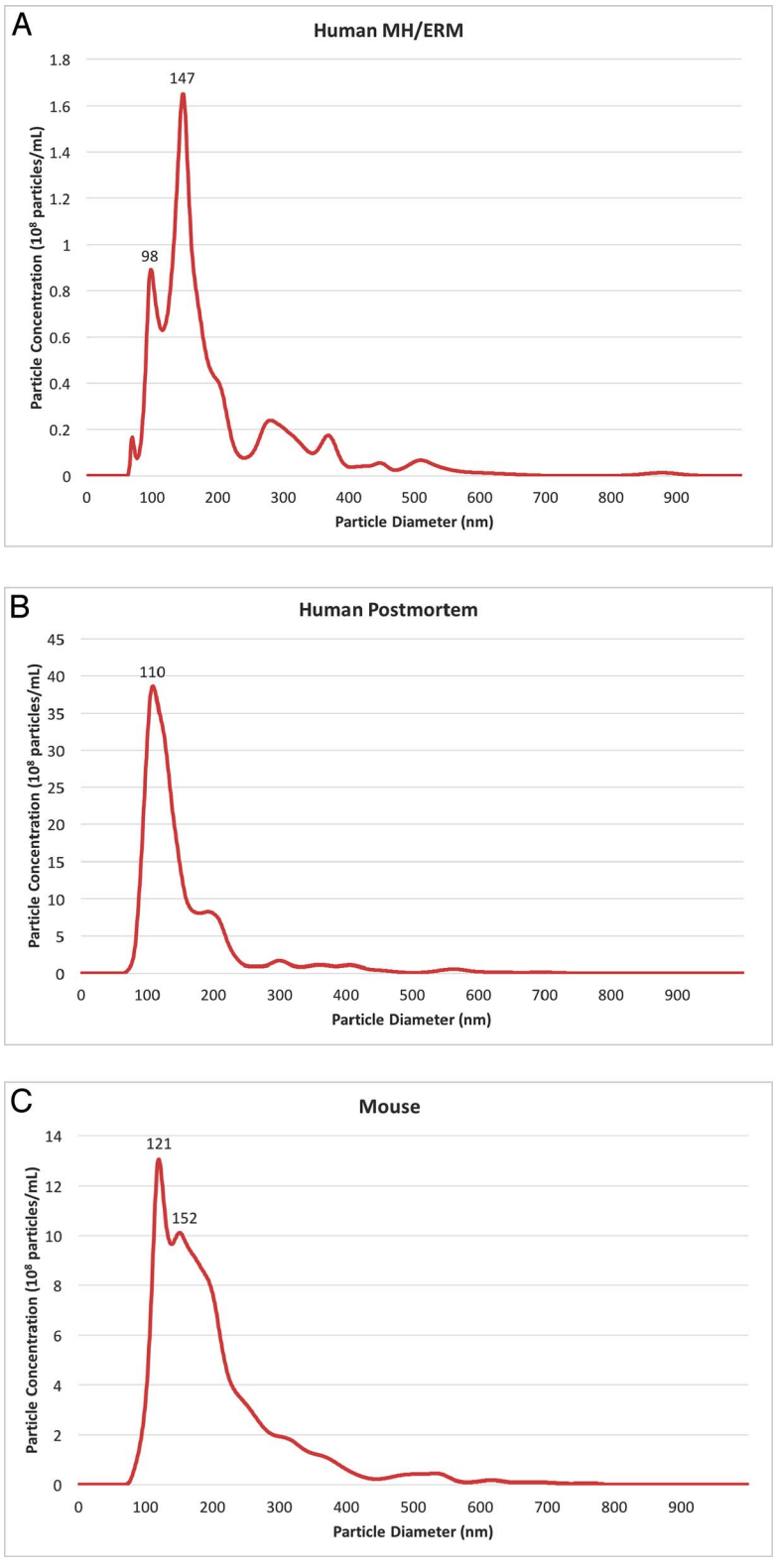

Figure 6. NanoSight analysis of unfractionated vitreous. NTA of vitreous humor from three sources revealed an average particle diameter of 123 nm when examining dominant peaks, defined as those constituting >5% of the total particles per sample. Average particle diameter is consistent across all three sample types, while particle concentrations vary substantially. Representative graphs are shown here; peaks constituting >5% of the data are labeled with their respective mean diameters. (A) Human vitreous from an MH/ERM patient reveals two peaks at diameters of 98 and 147 nm at concentrations of 9.1 and 17.4 × 10^8 particles/mL, respectively. (B) Human

←
postmortem vitreous is characterized by a peak at a similar diameter of 110 nm, but a significantly higher concentration of 415.7×10^8 particles/mL, a difference that can be attributed to artifact resulting from multiple hours of poor perfusion prior to harvesting. (C) Mouse vitreous shows two peaks at diameters of 121 and 152 nm, with concentrations of 138.4 and 110.5×10^8 particles/mL, an amount intermediate between that of the MH/ERM and postmortem human samples.

Further, 20 of the "Retinal Disease" proteins identified in the vitreous have previously been identified in exosomes (ExoCarta), suggesting that exosomes may play a role in the certain disease processes. While some of these proteins are plasma derived (complement components, APO-E, kininogen), others (retinoschisin, arrestin, VEGF, VEGF-R1, DDR1, EFEMP1) are known to be derived from retinal and/or RPE cells. Not only does this analysis provide one possibility for the origin of vitreal exosomes, but it also suggests that the processes occurring at the vitreoretinal interface are more complex than previously understood and that, consequently, the vitreous may be able to serve as a proximal biofluid of the retina.

Future studies will be required to determine if vitreous vesicle concentration and/or content is altered in retinal disease, but studies published in recent years support this possibility. For example, a recent study by Klingeborn et al.[43] examined the vitreous of patients with proliferative DR and proposed that RPE-derived exosomes are apically released and altered in the disease state. As mentioned previously, a report by Ragusa et al.[25] suggested that differences in the miRNA content of uveal melanoma vitreous relative to that of controls are due to exosome dysregulation. Together, these investigations further support the concept that exosomes may be altered in retinal disease.

Moreover, recent studies have shown therapeutic effects of intravitreal administration of exosomes themselves. Specifically, Moisseiv et al.[44] demonstrated that the administration of exosomes significantly reduced both retinal thinning and neovascularization in a model of oxygen-induced retinopathy, while Mead and Tomarev[45] found that intravitreal injection of exosomes derived from human mesenchymal stem cells promoted ganglion cell preservation in a model of optic nerve injury. These findings provide a solid framework for future investigation regarding a potential therapeutic role for intravitreal exosome administration in the treatment of retinal disease.

Thus, the presence of exosomes in vitreous, evidence that the vitreous proteome changes in a manner reflective of retinal disease, and the ability of exosomes administered into the vitreous to affect the retinal disease state strongly implicate vitreous exosomes in both normal retinal physiology and retinal disease. These observations, along with the ability to identify pathway and molecule changes in the vitreous associated with retinal disease states via proteomic analysis, provide the biological plausibility required to conduct vitreous biopsies.[46,47] Importantly, future studies examining both early- and end-stage retinal disease using liquid vitreous biopsies obtained in the operating room and in clinic will allow direct identification of retinal disease mechanisms.

A limitation of this study is that vitreous samples were not enriched for exosomes prior to proteomic analysis. Although billions of exosomes are present in vitreous, their contents account only for a small amount of total vitreous protein mass. As such, unbiased proteomics of vitreous exosomes is currently not feasible due to the large vitreous volume that would be required. Another limitation of the current study is that individual variability in the vitreous proteome cannot be discerned, as the samples were pooled prior to analysis. Unfortunately, this was required in order to have sufficient protein for in-depth analysis across several preparative strategies. Future studies analyzing vitreous in individual patients will be required to better understand individual variation in vitreous protein content. Additional '-omic' studies will also be required to identify proteins found within exosomes specifically and to relate them to retinal disease states.

In summary, the results of the current study suggest that exosomes are a constitutive and abundant component of vitreous. Although the origin of these vesicles remains unclear, it is clear that the study of exosomes in the context of retinal disease will greatly accelerate the identification of pathophysiologic changes that occur in the disease state as well as expedite the detection of novel therapeutic targets. It is clear from the current data that the vitreous is a bona fide proximal biofluid of the retina, and that the implementation of liquid vitreous biopsies into clinical practice will facilitate an improved understanding of the biochemical processes underlying retinal disease, identification of novel therapeutic targets, and enhanced treatment parameters.

Table 3. Vitreous Proteins Associated with Retinal Disease; Well-studied Protein Coding Genes, Protein Names, and Associated Retinal Diseases

Gene Name	Protein Name	Retinal Disease per OMIM
ADAM9[a]	ADAM metallopeptidase domain 9	Cone–rod dystrophy
ALDH3A2	Aldehyde dehydrogenase 3 family member A2	Macular dystophy associated with Sjogren-Larsson
AMIGO2	Adhesion molecule with Ig like domain 2	Atypical retinitis pigmentosa
ANXA2[a]	Annexin A2	Retinopathy associated with Waldenstrom Macroglobulinema
APOB[a]	Apolipoprotein B	Retinitis pigmentosa associated with familial hypobetalipoproteinemia
APOE	Apolipoprotein E	AMD; Sub-RPE deposit
C3	Complement C3	AMD; Sub-RPE deposit
CDH23	Cadherin related 23	Usher syndrome
CDHR1	Cadherin related family member 1	Cone–rod dystrophy 15; retinitis pigmentosa 65
CFH[a]	Complement factor H	AMD 4; basal laminar drusen
CFI[a]	Complement factor I	AMD 13
CHRDL1	Chordin-like 1	Megalocornea-1
COL18A1[a]	Collagen type XVIII alpha 1 chain	Knobloch syndrome-1
COL2A1[a]	Collagen type II alpha 1 chain	Stickler syndrome
EFEMP1[a]	EGF containing fibulin like extracellular matrix protein 1	Doyne honeycomb retinal dystrophy
EYS[a]	Eyes shut homolog (Drosophila)	Retinitis pigmentosa 25
FLT1[a]	Fms related tyrosine kinase 1 (VEGF-R1)	Retinal vascular disease
GNB1[a]	G protein subunit beta 1	Retinal degeneration
GUSB[a]	Glucuronidase beta	mucopolysaccharidosis VII; retinal degeneration
IGF1	Insulin-like growth factor 1	Retinopathy of prematurity; DR
IGFBP3[a]	Insulin-like growth factor binding protein 3	Retinopathy of prematurity
IGFBP7[a]	Insulin-like growth factor binding protein 7	Retinal arterial macroaneurysm
IMPG2	Interphotoreceptor matrix proteoglycan 2	Macular dystrophy, vitelliform, 5; retinitis pigmentosa 56
KDR	Kinase insert domain receptor	Retinal vascular diseases
MERTK	MER proto-oncogene, tyrosine kinase	Retinitis pigmentosa 38
MFRP	Membrane frizzled-related protein	Microphthalmia, isolated 5; nanophthalmos 2
MYOC[a]	Myocilin	Glaucoma 1A
PCDH15	Protocadherin-related 15	Usher syndrome type 1D/F; rode–cone degeneration
PLOD1[a]	Procollagen-lysine,2-oxoglutarate 5-dioxygenase 1	Ehlers-Danlos syndrome; retinal detachment
PPT1	Palmitoyl-protein thioesterase 1	Retinal degeneration associated with infantile neuronal ceroid llipofuscinosis

Table 3. Continued

Gene Name	Protein Name	Retinal Disease per OMIM
PRNP	Prion protein	Gerstmann-Straussler disease; optic atrophy
RBP3	Retinol binding protein 3	Retinitis pigmentosa 66
RBP4[a]	Retinol binding protein 4	Retinal dystrophy; iris coloboma; micropthalmia
RCVRN	Recoverin	Autoimmune petinopathy
RS1	Retinoschisin 1	X-linked petinoschisis
SAG	S-antigen visual arrestin	Oguchi disease-1; retinitis pigmentosa 47
SERPINF1[a]	Serpin family F member 1	Retinal detachment associated with osteogenesis imperfecta type VI; retinal development
SMOC1	SPARC-related modular calcium binding 1	Microphthalmia; retinal atrophy
SMPD1	Sphingomyelin phosphodiesterase 1	Retinal degeneration associated with Niemann-Pick type B
SOD1[a]	Superoxide dismutase 1	AMD
SOD2	Superoxide dismutase 2	Microvascular complications of diabetes
TPP1[a]	Tripeptidyl peptidase 1	Neuronal ceroid lipofuscinosis 2; retinal degeneration

Manually verified retinal disease-associated proteins that were present in the current vitreous samples are listed.
[a] Those that have also been identified in exosomes.

Acknowledgments

The authors thank Roland Myers, Penn State Hershey Imaging and Histology Core Facility, whose expertise was invaluable in collecting the TEM data.

Support generously provided by the Bennett and Inez Chotiner Early Career Professorship in Ophthalmology.

Disclosure: **Y. Zhao**, None; **S.R. Weber**, None; **J. Lease**, None; **M. Russo**, None; **C.A. Siedlecki**, None; **L.-C. Xu**, None; **H. Chen**, None; **W. Wang**, None; **M. Ford**, None; **R. Simó**, None; **J.M. Sundstrom**, None

References

1. Virgili G, Parravano M, Menchini F, Brunetti M. Antiangiogenic therapy with anti-vascular endothelial growth factor modalities for diabetic macular oedema. *Cochrane Database Syst Rev*. 2012;12:CD007419.
2. Diabetic Retinopathy Clinical Research Network,Wells JA, Glassman AR, et al. Aflibercept, bevacizumab, or ranibizumab for diabetic macular edema. *N Engl J Med*. 2015;372:1193–1203.
3. Solomon SD, Lindsley K, Vedula SS, Krzystolik MG, Hawkins B.S. Anti-vascular endothelial growth factor for neovascular age-related macular degeneration. *Cochrane Database Syst Rev*. 2014;8:CD005139.
4. Rofagha S, Bhisitkul RB, boyer DS, Sadda SR, Zhang K; for the SEVEN-UP Study Group. Seven-year outcomes in ranibizumab-treated patients in ANCHOR, MARINA, and HORIZON: a multicenter cohort study (SEVEN-UP). *Ophthalmology*. 2013;120:2292–2299.
5. Sebag J. Ageing of the vitreous. *Eye*. 1987;1(Pt 2):254–262.
6. Pischel DK. Detachment of the vitreous as seen with slit-lamp examination. *Trans Am Ophthalmol Soc*. 1952;50:329–346.
7. Duker JS, Kaiser PK, Binder S, et al. The International Vitreomacular Traction Study Group classification of vitreomacular adhesion, traction, and macular hole. *Ophthalmology*. 2013;120:2611–2619.
8. Kim T, Kim SJ, kim K, et al. Profiling of vitreous proteomes from proliferative diabetic retinopathy and nondiabetic patients. *Proteomics* 2007;7:4203–4215.

9. Aretz S, Krohne TU, Kammerer K, et al. In-depth mass spectrometric mapping of the human vitreous proteome. *Proteome Sci*. 2013;11:22.
10. Murthy KR, Goel R, Subbannayya Y, et al. Proteomic analysis of human vitreous humor. *Clin Proteomics*. 2014;11:29.
11. Skeie JM, Roybal CN, Mahajan VB. Proteomic insight into the molecular function of the vitreous. *PLoS One*. 2015;10:e0127567.
12. Rocha AS, Santos FM, Monteiro JP, et al. Trends in proteomic analysis of human vitreous humor samples. *Electrophoresis*. 2014;35:2495–2508.
13. Lopez-Verrilli MA, Court FA. Exosomes: mediators of communication in eukaryotes. *Biol Res*. 2013;46:5–11.
14. Gallo A, Tandon M, Alevizos I, Illei GG. The majority of microRNAs detectable in serum and saliva is concentrated in exosomes. *PLoS One*. 2012;7:e30679.
15. Valadi, H, Ekstrom K, Bossios A, Sjostrand M, Lee JJ, lotall JO. Exosome-mediated transfer of mRNAs and microRNAs is a novel mechanism of genetic exchange between cells. *Nat Cell Boil*. 2007;9:654–659.
16. Mathivanan S, Ji H, Simpson RJ. Exosomes: extracellular organelles important in intercellular communication. *J Proteomics*. 2010;73:1907–1920.
17. Skeie JM, Tsang SH, Mahajan VB. Evisceration of mouse vitreous and retina for proteomic analyses. *J Vis Exp*. 2011:e2795.
18. Hulleman JD, Brown SJ, Rosen H, Kelly JW. A high-throughput cell-based Gaussia luciferase reporter assay for identifying modulators of fibulin-3 secretion. *J Biomol Screen*. 2013;18:647–658.
19. Thery C, Amigorena S, Raposo G, Clayton A. Isolation and characterization of exosomes from cell culture supernatants and biological fluids. *Curr Protoc Cell Biol*. 2006; Chapter 3: Unit 3.22.
20. Simpson RJ, Kalra H, Mathivanan S. ExoCarta as a resource for exosomal research. *J Extracell Vesicles*. 2012:1.
21. Sharma S, Rasool HI, palanisamy V, et al. Structural-mechanical characterization of nanoparticle exosomes in human saliva, using correlative AFM, FESEM, and force spectroscopy. *ACS Nano*. 2010;4:1921–1926.
22. Lotvall J, Hill AF, Hochberg F, et al. Minimal experimental requirements for definition of extracellular vesicles and their functions: a position statement from the International Society for Extracellular Vesicles. *J Extracell Vesicles*. 2014;3:26913.
23. Colombo M, Raposo G, Thery C. Biogenesis, secretion, and intercellular interactions of exosomes and other extracellular vesicles. *Ann Rev Cell Dev Biol*. 2014;30:255–289.
24. Charras GT. A short history of blebbing. *J Microsc*. 2008;231:466–478.
25. Ragusa M, Barbagallo C, Statello L, et al. miRNA profiling in vitreous humor, vitreal exosomes and serum from uveal melanoma patients: Pathological and diagnostic implications. *Cancer Biol Ther*. 2015;16:1387–1396.
26. Dismuke WM, Challa P, Navarro I, Stamer WD, Liu Y. Human aqueous humor exosomes. *Exp Eye Res*. 2015;132:73–77.
27. Kang GY, Bang JY, Choi AJ, et al. Exosomal proteins in the aqueous humor as novel biomarkers in patients with neovascular age-related macular degeneration. *J Proteome Res*. 2014;13:581–595.
28. Lerner N, Avissar S, Beit-Yannai E. Extracellular vesicles mediate signaling between the aqueous humor producing and draining cells in the ocular system. *PLoS One*. 2017;12:e0171153.
29. Hoffman EA, Perkumas KM, Highstrom LM, Stamer WD. Regulation of myocilin-associated exosome release from human trabecular meshwork cells. *Invest Ophthalmol Vis Sci*. 2009;50:1313–1318.
30. Atienzar-Aroca S, Flore-Bellver M, Serrano-Heras G, et al. Oxidative stress in retinal pigment epithelium cells increases exosome secretion and promotes angiogenesis in endothelial cells. *J Cell Mol Med*. 2016;20,:1457–1466.
31. Biasutto L, Chiechi A, Couch R, Liotta LA, Espina V. Retinal pigment epithelium (RPE) exosomes contain signaling phosphoproteins affected by oxidative stress. *Exp Cell Res*. 2013;319:2113–2123.
32. Wang AL, Lukas TJ, Yuan M, Du N, Tso MO, Neufeld AH. Autophagy and exosomes in the aged retinal pigment epithelium: possible relevance to drusen formation and age-related macular degeneration. *PLoS One*. 2009;4:e4160.
33. Grigor'eva, A.E, Tamkovich SN, Ermina AV, et al. Characteristics of exosomes andmicroparticles discovered in human tears [in Russian]. *Biomed Khim*. 2016;62:99–106.
34. Sadeghipour S, Mathias RA. Herpesviruses hijack host exosomes for viral pathogenesis. *Semin Dev Cell Biol*. 2017;67:91–100.
35. Smith VL, Cheng Y, Bryant BR, Schorey JS. Exosomes function in antigen presentation during

an in vivo Mycobacterium tuberculosis infection. *Sci Rep*. 2017;7:43578.
36. Rajendran L, Honsho M, Zahn TR, et al. Alzheimer's disease beta-amyloid peptides are released in association with exosomes. *Proc Natl Acad Sci U S A*. 2006;103:11172–11177.
37. Abner EL, Jicha GA, Shaw LM, Trojanowski JQ, Goetzl EJ. Plasma neuronal exosomal levels of Alzheimer's disease biomarkers in normal aging. *Ann Clin Transl Neurol*. 2016;3:399–403.
38. Yuyama, K, Sun H, Usuki S, et al. A potential function for neuronal exosomes: sequestering intracerebral amyloid-beta peptide. *FEBS Lett*. 2015;589:84–88.
39. Kore RA, Abraham EC. Inflammatory cytokines, interleukin-1 beta and tumor necrosis factor-alpha, upregulated in glioblastoma multiforme, raise the levels of CRYAB in exosomes secreted by U373 glioma cells. *Biochem Biophys Res Commun*. 2014;453:326–331.
40. Eldh M, Olofsson Gagge R, Lasser C, et al. MicroRNA in exosomes isolated directly from the liver circulation in patients with metastatic uveal melanoma. *BMC Cancer*. 2014;14:962.
41. Zhang H, Deng T, Liu R, et al. Exosome-delivered EGFR regulates liver microenvironment to promote gastric cancer liver metastasis. *Nat Commun*. 2017;8:15016.
42. Isola AL, Chen S. Exosomes: the messengers of health and disease. *Curr Neuropharmacol*. 2017; 15:157–165.
43. Klingeborn M, Dismuke WM, Bowes Rickman C, Stamer WD. Roles of exosomes in the normal and diseased eye. *Prog Retin Eye Res*. 2017;59: 158–177.
44. Moisseiev, E, Anderson JD, Oltjen S, et al. Protective effect of intravitreal administration of exosomes derived from mesenchymal stem cells on retinal ischemia. *Curr Eye Res*. 2017;42:1358–1367.
45. Mead B, Tomarev S. Bone marrow-derived mesenchymal stem cells-derived exosomes promote survival of retinal ganglion cells through miRNA-dependent mechanisms. *Stem Cells Transl Med*. 2017;6:1273–1285.
46. Gardner TW, Sundstrom JM. A proposal for early and personalized treatment of diabetic retinopathy based on clinical pathophysiology and molecular phenotyping. *Vision Res*. 2017;139: 153–160.
47. Ghodasra DH, Fante R, gardener TW, et al. Safety and feasibility of quantitative multiplexed cytokine analysis from office-based vitreous aspiration. *Invest Ophthalmol Vis Sci*. 2016;57: 3017–3023.